Journal of Power Sources 228 (2013) 112–119

Contents lists available at SciVerse ScienceDirect

Journal of Power Sources

journal homepage: www.elsevier.com/locate/jpowsour

Graphite microspheres decorated with Si particles derived from waste solid of organosilane industry as high capacity anodes for Li-ion batteries

Jing Yu [a,b], Hanhui Zhan [a,**], Yanhong Wang [b,*], Zailiei Zhang [b], Han Chen [b], Hong Li [c], Ziyi Zhong [d], Fabing Su [b,*]

[a] School of Environment Science and Spatial Informatics, China University of Mining and Technology, Xuzhou 221116, PR China
[b] State Key Laboratory of Multiphase Complex Systems, Institute of Process Engineering, Chinese Academy of Sciences, Beijing 100190, PR China
[c] Institute of Physics, Chinese Academy of Sciences, Beijing 100190, PR China
[d] Institute of Chemical Engineering and Sciences, A*star, 1 Pesek Road, Jurong Island, Singapore 627833, Singapore

HIGHLIGHTS

- Si waste from organosilane industry was used for preparation of Si/C composite.
- Graphite microspheres were decorated with Si particles and sucrose as the binder.
- The Si/C composite anodes show the enhanced electrochemical performance.

ARTICLE INFO

Article history:
Received 6 October 2012
Received in revised form
21 November 2012
Accepted 23 November 2012
Available online 30 November 2012

Keywords:
Silicon waste
Graphite
Silicon/carbon composite anode
Lithium-ion batteries
Electrochemical performance

ABSTRACT

We report the decoration of commercial graphite microspheres (GMs) with Si particles as anode materials for Li-ion batteries. The Si particles are obtained from solid Si waste of organosilane industry that is acid-washed to remove the impurities and further ground. The GMs with a size of 5–40 μm as main active material, Si particles with a size of 1–10 μm as an additive, and sucrose dissolved in water as a binder are mixed and followed by carbonization to obtain Si/C composites containing graphite, Si, and amorphous carbon generated from sucrose. It is found that the composite containing 60.5 wt% of GMs, 22.1 wt% of Si, and 17.4 wt% of amorphous carbon obtained at 800 °C for 5 h shows the best electrochemical performance with a specific capacity of 522.6 mA h g^{-1} at the current density of 50 mA g^{-1} and 306.9 mA h g^{-1} at 500 mA g^{-1}, much higher than those of GMs. Its capacity retention at 500 mA g^{-1} attains 93.9% after 20 cycles. The work demonstrates the possibility for utilization of the industrial Si waste to enhance graphite anode materials in Li-ion batteries.

1. Introduction

In recent years, many efforts have been undertaken to improve the Li-ion battery materials by designing and utilizing various nanostructured composite materials possessing high energy density and good cyclability. Si is considered as a promising next-generation anode material because of its much higher theoretical specific capacity (4200 mA h g^{-1}) than that of the commercial graphite anode (ca. 372 mA h g^{-1}) [1–3]. However, the use of Si has been hindered by its poor cycling performance due to its low intrinsic electric conductivity and severe volume change during Li alloying/dealloying processes, which causes pulverization of electrode [4–7]. There are mainly four ways to improve the Si anode electrode for lithium ion batteries: (1) fabricating nanostructured Si materials; (2) surface coating; (3) improving the electrolyte; (4) improving the current collector. Therefore, in recent years many attempts have been carried out to develop the various nanostructured Si anode materials to accommodate the volume changes [8–11], such as Si nanocrystals [12,13], nanowires [14–20], nanotubes [21–23], nanorods [24], films [25,26], hollow nanospheres [10,27], and porous Si [28,29]. However, the essential technical barrier of the severe pulverization of the active Si derived from its volume expansion has not been successfully overcome.

The application of Si/C composites is regarded as an effective route to improve the anode performance, and carbon could be able to alleviate the volume change and mechanical stress [30,31], while

* Corresponding authors. Tel.: +86 10 82544850; fax: +86 10 82544851.
** Corresponding author.
E-mail addresses: zhanhhh@263.net (H. Zhan), wangyanhong@mail.ipe.ac.cn (Y. Wang), fbsu@mail.ipe.ac.cn (F. Su).

0378-7753/$ – see front matter © 2012 Elsevier B.V. All rights reserved.
http://dx.doi.org/10.1016/j.jpowsour.2012.11.083

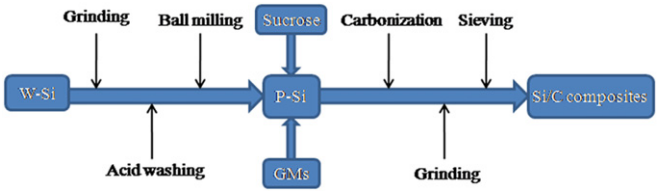

Scheme 1. Preparation scheme of Si/C composites.

increasing the electronic conductivity of the electrode composites [31]. A cage-like CNTs/Si composite was formed by Shu et al. [23], where coiled carbon nanotubes were grown on small Si particles forming a cage to enwrap Si particles tightly, and it showed better cyclic performance. It was reported that high-performance Si/C anodes were synthesized via chemical vapor deposition (CVD) using SiH_4 as the Si precursor and C_3H_6 as the carbon precursor [32]. Park et al. [33] prepared Si/C nanotube composite anodes by reductive decomposition of a Si precursor in an alumina template followed by carbon deposition. Kim et al. [34] prepared good Si/C anode material containing carbon coated 10 nm Si nanoparticles generated from $SiCl_4$ using reverse micelles under high temperature and pressure. Holzapfel et al. [35] produced Si/graphite anode composites by pyrolysis of SiH_4, which showed good reversible lithium insertion. Si@SiO_x/C [1] and Si/C nanocomposites [36] could be obtained by hydrothermal carbonization of glucose in the presence of Si nanoparticles, or by spray-pyrolysis process using Si nanoparticles and organic solvent as the precursors [37]. In addition, other Si/C composite anodes, such as carbon nanofibers embedded with Si nanoparticles [38], Si-coated carbon nanowires by CVD [39], and carbon-coated Si nanowires synthesized by supercritical fluid–liquid–solid method [19], are also reported. These results demonstrate that the combination of graphitic carbon with Si particles can generate high performance Si/C composite anodes [36–38]. However, there is still a long way to the commercial use of these Si-based anodes due to their unsatisfied properties, complicated synthesis process and high cost. More recently, Chang et al. [40] demonstrated the use of cheap quartz powders to fabricate Si anodes with nanosized Si embedded in amorphous silica through a high energy mechanical milling method, providing a cost-effective route to Si-based anode materials.

Herein, we report the preparation of Si/C composite anodes containing commercial graphite microspheres (GMs), Si particles, and amorphous carbon (AC) generated from the sucrose. The low cost Si particles were obtained from the waste Si solid of organosilane industry. The direct synthesis of methylchlorosilanes via reaction of Si powder with chloromethane over the copper-based catalysts, although discovered by Rochow as early as in 1940s [41], is still the most economical route in organosilane industry. In this process, a large amount of solid waste composed of 10–30 wt% of copper compounds and 70–90 wt% of Si is inevitably produced due to the limitations of reaction kinetics and reactors. Generally, these solid wastes are treated by acid dissolution followed by precipitation with alkaline solution to recover the copper compounds, but the residual Si particles have not found the high value utilization. This work attempts to prepare Si/C anode materials using these low cost Si particles by simply mixing them with graphite microspheres and sucrose followed by carbonization. GMs and AC in composites could act as a buffer matrix for Li–Si alloy during cycling [42]. In addition, AC can effectively bind Si with GMs forming the electrical conductive network [43–45]. The Si/C composite obtained under the optimized condition shows good electrochemical performance. The work provides a promising solution to the value-added application of the residual Si particles and to the preparation of low cost Si/C composite anodes for Li-ion batteries.

Table 1
Synthesis conditions of all the Si/C anode materials.

Entry	Sample	GMs (g)	Si (g)	Sucrose (g)	Temperature (°C)	Time (h)
1	Si/C-700	0.9	0.3	1.2	700	5
2	Si/C-800-1	0.9	0.3	0.3	800	5
3	Si/C-800-2	0.9	0.3	1.2	800	5
4	Si/C-800-3	0.9	0.3	1.8	800	5
5	Si/C-900	0.9	0.3	1.2	900	5
6	Si/C-1000	0.9	0.3	1.2	1000	5

Table 2
Elemental analysis of W-Si and P-Si.

Sample	Si (%)	O (%)	Cu (%)	Fe (%)	Cl (%)	Ca (%)	Al (%)
W-Si	34.5	24.1	20.8	10.6	3.9	1.6	1.4
P-Si	96.5	2.3	<0.1	0.7	<0.1	0.2	0.2

2. Experimental

2.1. Preparation

The waste Si, named as W-Si, was provided by Jiangsu Hongda New Material Co., Ltd. The preparation of Si/C composites is illustrated in Scheme 1. Firstly, W-Si was ground with a high-speed universal disintegrator (FW80, Tianjin Taisite Instrument Co., LTD) to obtain the fine powders followed by washing with nitric acid solution (HNO_3, A.R., Beijing Chemical Works) to remove the metal impurities. After filtration and water-washing, the Si particles were then milled with planetary ball mill (QM-3SP04, Nanjing University Instrument Plant) and sieved to obtain purified Si particles (≥200

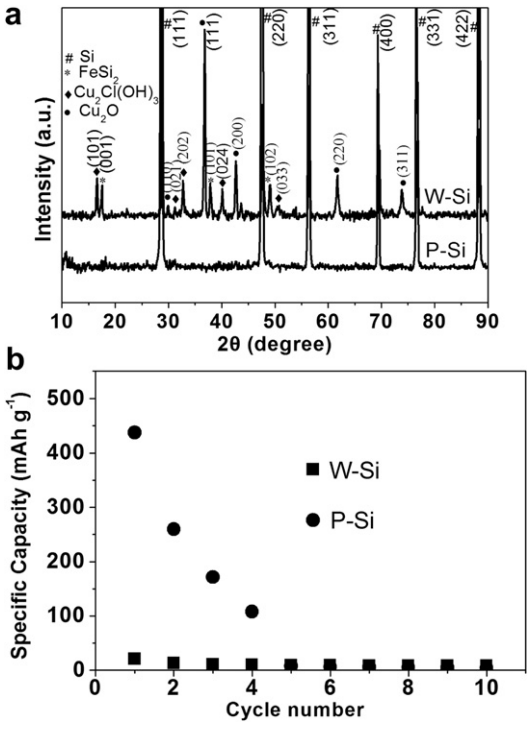

Fig. 1. XRD patterns (a) and charge specific capacity at 50 mA g^{-1} (b) of W-Si and P-Si.

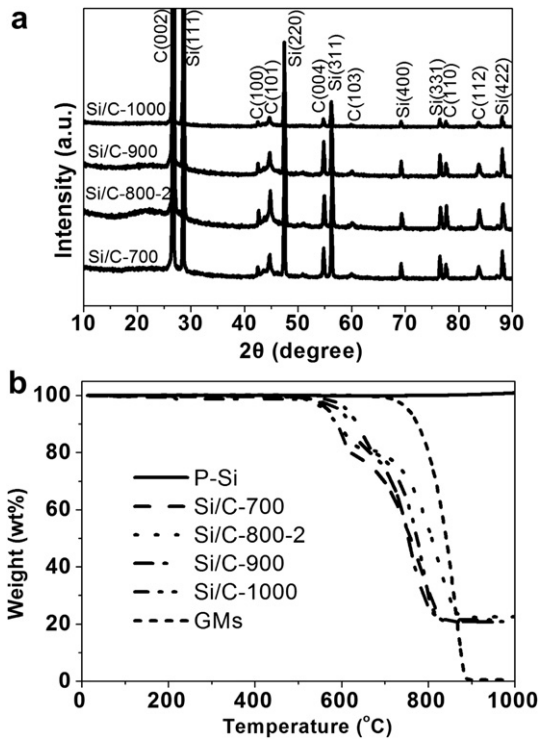

Fig. 2. XRD patterns (a) and TG curves (b) of Si/C samples carbonized at different temperatures.

mesh), named as P-Si. The synthesis parameters of Si/C composites were compiled in Table 1. In a typical procedure, for example, Si/C-700 sample, 1.2 g sucrose ($C_{12}H_{22}O_{11}$, A.R., Xilong Chemical Co., Ltd.) was dissolved in 10 mL deionized water and mixed with 0.3 g of P-Si and 0.9 g of GMs (Qingdao Tianhe Graphite Co., Ltd., China). The mixture was dried at 60 °C under stirring and further carbonized at 700 °C for 5 h in an argon flow. Finally, the carbonized product was ground, sieved (≥200 mesh), and denoted as Si/C-700 composite.

2.2. Characterization

The elemental analysis experiment was conducted by X-ray fluorescence (XRF) (PANalytical Axios). X-ray diffraction (XRD) patterns were recorded on a PANalytica X'Pert PRO MPD using the Kα radiation of Cu. The crystal size of the sample was calculated using the Debye–Scherrer equation. The particle size distribution (PSD) was measured by Laser Particle Size Analyzer (BT-9300Z, Bettersize Instruments Ltd., China). The microscopic feature was observed by field-emission scanning electron microscopy (SEM) (JSM-6700F, JEOL, Tokyo, Japan) and transmission electron microscopy (TEM) (JEM-2010F, JEOL, Tokyo, Japan). The surface composition of the samples was investigated by X-ray photoelectron spectroscopy (XPS) using an ESCALab250 electron spectrometer from Thermo Scientific Corporation with monochromatic 150 W Al Kα radiation. Thermogravimetric (TG) analysis was carried out on an EXSTAR TG/DTA 6300 instrument (Seiko Instruments, Japan) with a heating rate of 10 °C min^{-1} in air.

2.3. Electrochemical measurement

The working electrodes were prepared by mixing Si/C active materials, acetylene black, and polyvinylidene fluoride (PVDF) with a weight ratio of 75:15:10 using N-methylpyrrolidone (NMP) as the solvent. The resulting slurry was cast onto copper current collectors and then dried at 120 °C under vacuum for 24 h. The foils were rolled into sheets with a thickness of 30 μm, and then cut into disks with a diameter of 14 mm. R2016 coin-type cells were assembled with lithium foils as counter electrodes and polypropylene

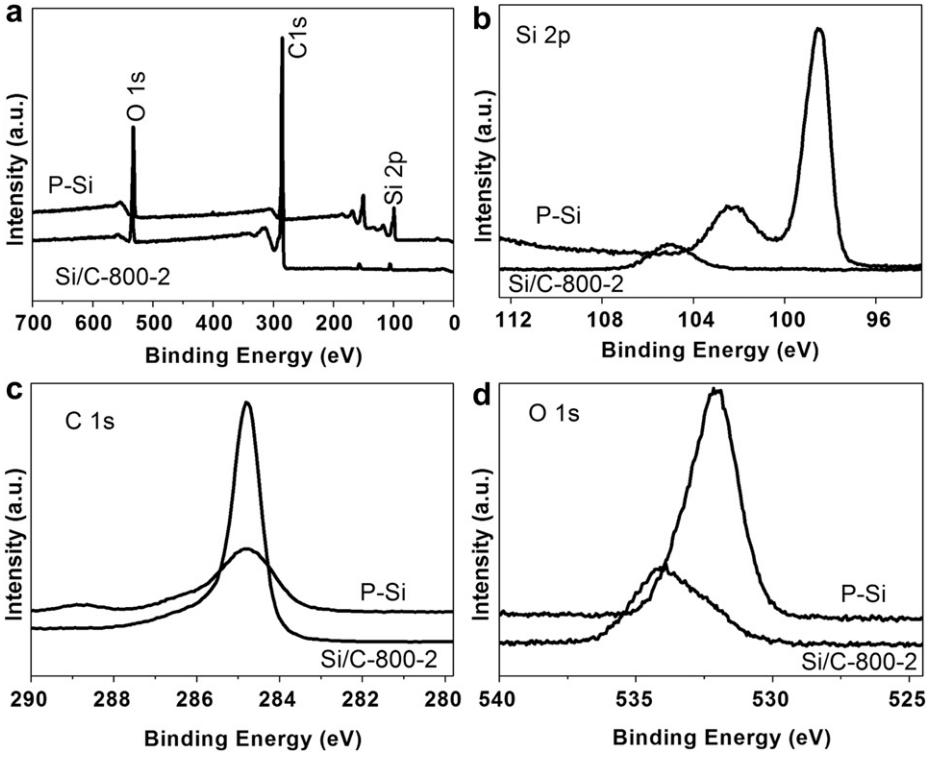

Fig. 3. XPS spectra of P-Si and Si/C-800-2: (a) Wide spectrum, (b) Si 2p, (c) C 1s, and (d) O 1s.

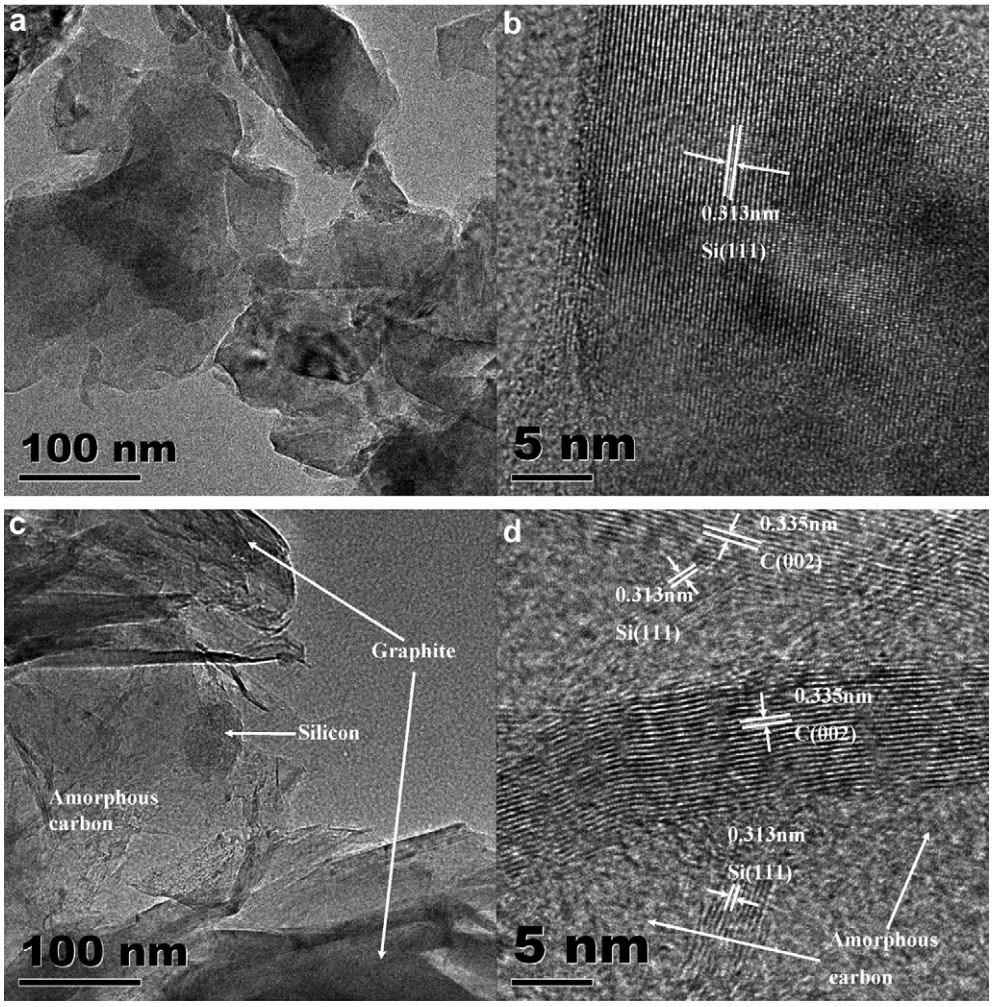

Fig. 4. TEM images of P-Si (a and b) and Si/C-800-2 (c and d).

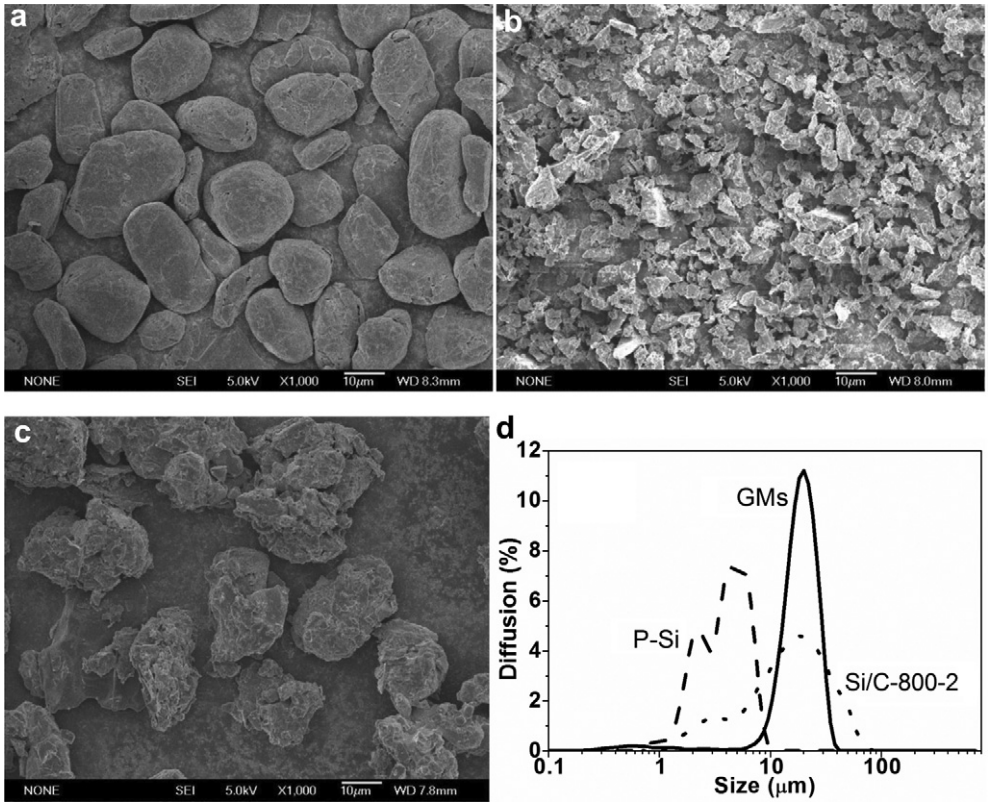

Fig. 5. SEM images of GMs (a), P-Si (b), and Si/C-800-2 (c), and PSD curves of P-Si, GMs, and Si/C-800-2 (d).

microporous films (Celgard 2400) as separators in an argon-filled glove box. The liquid electrolyte with 1 mol L^{-1} $LiPF_6$ in a mixture of ethylene carbonate (EC) and dimethyl carbonate (DMC) (1:1, v/v) was used. The galvanostatic charge and discharge tests were carried out by CT2001A LAND testing instrument in a potential range between 0.01 and 2.00 V with various current rates at room temperature. Electrochemical impedance spectroscopy (EIS) measurements were also carried out on this instrument in the frequency range from 100 kHz to 10 mHz at an ac oscillation of 5 mV.

3. Results and discussion

Besides element Si, W-Si derived from the solid residue of Rochow reaction in organosilane industry contains many impurities. Table 2 shows the XRF analytic results of W-Si and P-Si. For W-Si, the content of Si, O, Cu and Fe is 34.5, 24.1, 20.8 and 10.6 wt%, respectively. The high content of Cu and Fe in W-Si stems from the copper-based catalyst and the Si raw materials, respectively. After the acid-washing treatment, the Si content in P-Si is 96.5 wt%, much higher than that of W-Si, suggesting its high purity. The O content is 2.3 wt%, probably due to the presence of SiO_x film on the surface of P-Si.

Fig. 1a shows the XRD patterns of W-Si and P-Si. The peaks observed at about 28.3°, 47.1°, 55.9°, 68.9°, 76.3° and 87.9° correspond to (111), (220), (311), (400), (331) and (422) diffractions of Si (JCPDS NO. 27-1402), respectively. Besides the Si diffraction peaks in W-Si, the other diffraction peaks can be indexed as $FeSi_2$, $Cu_2Cl(OH)_3$, and Cu_2O. However, in the XRD pattern of P-Si, all peaks are solely assigned to Si, further indicating the high efficiency of the acid treatment in removal of all impurities. Fig. 1b shows cycling performance curves of W-Si and P-Si at 50 mA g^{-1}. Half-cells were assembled in the experiment, so the discharge process means the Li alloying reaction with Si, and charge process means the de-alloying of Li from Li–Si alloy. The initial charge specific capacity of W-Si is only 20.6 mA h g^{-1}, much lower than that of P-Si (437.7 mA h g^{-1}). After 5 cycles, both samples almost have no capacity, suggesting their much poor electrochemical properties.

Fig. 2a shows XRD patterns of the Si/C samples carbonized at different temperatures. The peaks observed at about 26.7°, 42.6°, 44.8°, 54.8°, 60.0°, 77.6° and 83.7° correspond to (002), (100), (101), (004), (103), (110) and (112) diffractions of graphite carbon (JCPDS NO. 25-0284), respectively. The calculated crystal size of graphite is 52.2, 59.0, 55.5, and 57.5 nm for Si/C4-700, Si/C4-800-2, Si/C4-900, and Si/C4-1000, respectively. The group peaks at about 28.3°, 47.1°, 55.9°, 68.9°, 76.3° and 87.9° are assigned to (111), (220), (311), (400), (331) and (422) diffractions of Si (JCPDS NO. 27-1402), respectively. The calculated Si crystal size of Si/C-700, Si/C-800-2, Si/C-900, and Si/C-1000 is 55.7, 65.8, 68.0, and 78.3 nm, respectively, indicating P-Si is composed of polycrystals. In addition, there is no any other new peaks appeared after the carbonization. Fig. 2b shows the TG curves of Si/C samples carbonized at different temperatures. The TG curve of P-Si shows that there is a weight increase of about 0.2 wt% above 900 °C due to the formation of surface SiO_x film in air at high temperatures [1,46]. The combustion of GMs starts at 700 °C and completes at around 900 °C without any residue. The Si/C composites display two well-resolved weight losses [47]: the one in low temperature range between 500 and 670 °C is due to the combustion of AC, and the one in high temperature range between 670 and 880 °C is ascribed to the combustion of GMs. The weight of AC calculated roughly from the TG curves is about 17.4 wt% for the all Si/C samples. Assuming that the weight of Si and GMs has no big change after carbonization, the deduced weight ratio of GMs:Si:AC is nearly 3:1:1 in all four samples.

Fig. 3 presents the XPS spectra of P-Si and Si/C-800-2. Fig. 3a displays the wide XPS spectra of the two samples, suggesting the presence of only Si, C and O elements in them. In the Si 2p spectrum of P-Si spectrum shown in Fig. 3b, there is a strong Si peak at about 98.5 eV and a weak SiO_x peak at about 102.1 eV [48]. The presence of Si oxide is due to native oxide formation. However, for Si/C-800-2, there is only a weak peak at about 104.8 eV, without the observation of the Si signal. It is because in this sample the Si particles are covered with a carbon film, which is too thick to be penetrable. Fig. 3c presents the C 1s spectrum of both samples. For P-Si sample, the small peak of C1s at 284.8 eV may be due to the presence of carbon deposit formed during the organosilane synthesis [49]. For Si/C-800-2, the intensity of C 1s peak increases obviously, indicating the formation of carbon layers on the Si particles. The O 1s spectrum in Fig. 3d shows a strong O 1s peak for P-Si, implying the presence of SiO_x, consistent with XRF analysis. For Si/C-800-2, a relatively weak O 1s peak is observed, further demonstrating that the Si particles are covered with carbon.

Fig. 4 shows the TEM images of P-Si and Si/C-800-2. The irregular Si particles can be seen in Fig. 4a, and its high magnification

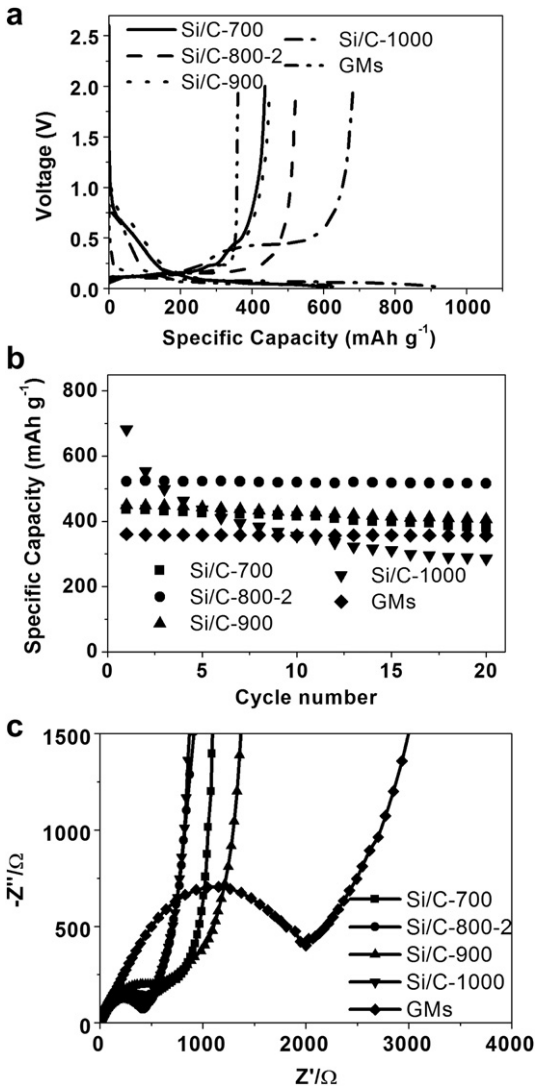

Fig. 6. Electrochemical performance of Si/C composites obtained at different carbonization temperatures: (a) Initial galvanostatic charge-discharge profiles at 50 mA g^{-1}, (b) charge specific capacity within 20 cycles at 50 mA g^{-1}, and (c) electrochemical impedance plots.

image in Fig. 4b reveals the well-resolved lattice planes with a distance of approximately 0.313 nm, corresponding to the (111) planes of the Si crystal. In the TEM images of Si/C-800-2 (Fig. 4c and d), Si particles, GMs, and flaky AC can be observed, showing Si and GMs are embedded in AC networks forming a Si/C composite.

Fig. 5a shows the SEM image of GMs. It can be seen that GMs possess a ellipsoidal morphology with a particle size of 5–40 μm. Fig. 5b shows a SEM image of P-Si irregular particles with a size of 1–10 μm, and Fig. 5c shows a SEM image of Si/C-800-2. The particles of Si/C-800-2 become larger than that of GMs and their surface is much coarser, suggesting that the P-Si particles are adhered to the surface of GMs with AC as a binder. Fig. 5d shows the PSD curves of these three samples. It can be seen that the particle size of GMs, P-Si, and Si/C-800-2 is located in the range of 6–40, 0.7–10, and 1–100 μm, respectively, consistent with the SEM observation. Some particle size of Si/C-800-2 is smaller than GMs, possibly because Si particles were partially peeled off from the GMs during the grinding process.

Fig. 6 presents the electrochemical performance curves of the Si/C composites obtained at different carbonization temperatures. Fig. 6a shows the initial galvanostatic charge–discharge curves at 50 mA g^{-1}. It can be seen that GMs exhibits a sloping voltage plateau between 0.75 and 0.20 V in the first discharge curve, linking to the formation of solid electrolyte interface (SEI) film on the surface of graphite [50]. There is a long and flat voltage plateau at 0.20 V, suggesting the insertion of lithium ions into graphite. During the charge process, GMs only show a long plateau around 0.1 V corresponding to the extraction of lithium ions from graphite. The initial discharge and charge specific capacity of GMs is 363.6 and 361.0 mA h g^{-1}, respectively. For Si/C-800-2 composite, a long sloping voltage plateau between 0.75 and 0.20 V can be seen during the first discharge process, corresponding to the formation of SEI on the surface of electrode, and then there is a long and flat voltage plateau below 0.20 V, suggesting the insertion of lithium ions in graphite and Si [50,51]. During the charge process, there are two voltage plateaus located at 0.10 and 0.30 V, corresponding to the extraction of lithium ions from graphite and de-alloying of $Li_{4.4}Si$ [11,51]. Compared with Si/C-800-2 composites, the initial discharge and charge capacities of GMs are lower, suggesting that the high specific capacity with Si/C-800-2 is caused by Li alloying reaction with Si particles. Accordingly, the initial charge specific capacity is 436.4 mA h g^{-1} for Si/C-700, 522.6 mA h g^{-1} for Si/C-800-2, 449.9 mA h g^{-1} for Si/C-900, and 682.7 mA h g^{-1} for Si/C-1000. The initial coulombic efficiency of Si/C-700, Si/C-800-2, Si/C-900, and Si/C-1000 is 71.6, 77.5, 70.0, and 72.9%, respectively, and among these composites, Si/C-800-2 exhibits the highest value. Fig. 6b shows the cycling performance curves of these composites at 50 mA g^{-1}. Si/C-1000 exhibits the highest initial charge specific capacity, but it decreases most rapidly, and the capacity retention is only 41.9% after 20 cycles. For other composites, after 20 cycles, the capacity retentions are 87.3% for Si/C-700, 98.8% for Si/C-800-2, and 90.2% for Si/C-900, and among them, Si/C-800-2 still shows the highest capacity retention, even as good as that of GMs (98.9%). More importantly, after 20 cycles, Si/C-800-2 still maintains the highest specific capacity (516.3 mA h g^{-1}) among these composites, much higher than that of GMs (357.0 mA h g^{-1}). Therefore, the carbonization temperature has a significant effect on the electrochemical performance of Si/C composites and 800 °C is the optimal carbonization temperature. Fig. 6c shows the electrochemical impedance plots of these samples. The samples all show one depressed semicircle in the high medium frequency region, which is related to the charge-transfer resistance on the electrode interface [52]. It should be pointed out that Si/C composites show much smaller semicircle than GMs, indicating a lower electrochemical reaction resistance in the Si/C composites electrode, probably because of the presence of conductive network created by AC generated from carbonization of sucrose.

According to the above results, Si/C composites carbonized at 800 °C with different AC amounts were further prepared. Fig. 7a shows the XRD patterns of these samples, in which all the peaks are indexed to Si and graphite, in good agreement with the observation of Fig. 2a. The TG curves of these Si/C composites are shown in

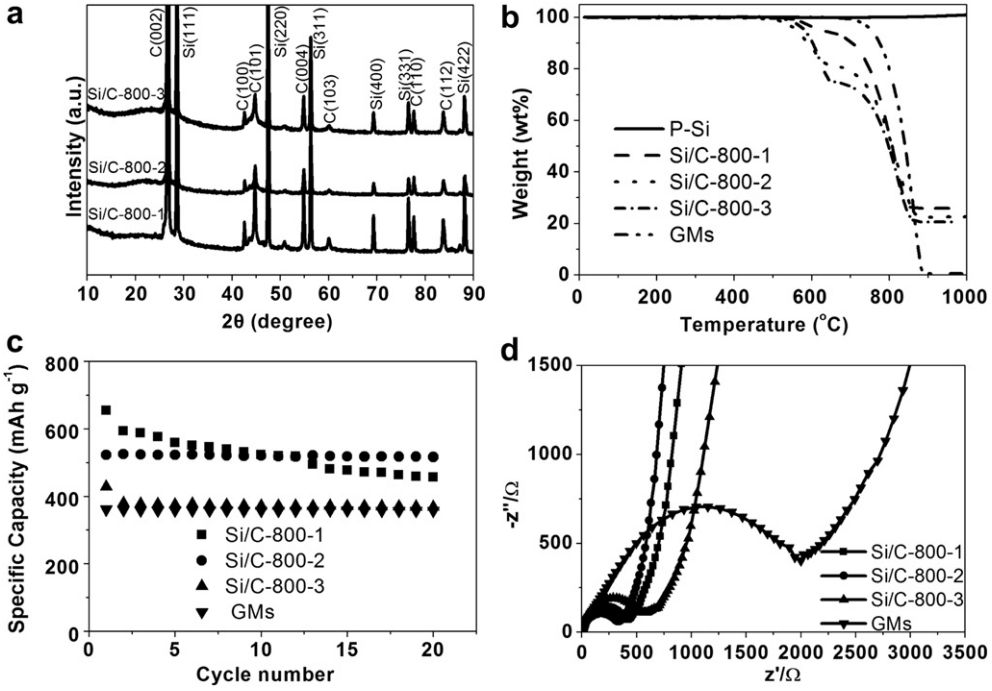

Fig. 7. XRD patterns (a), TG curves (b), charge specific capacity within 20 cycles at 50 mA g^{-1} (c), and electrochemical impedance plots (d) of Si/C composites carbonized at 800 °C with different AC content.

Fig. 7b. In Si/C-800-1, Si/C-800-2 and Si/C-800-3, the Si content is 25.9, 22.1, and 20.6 wt%, and AC content is 5.1, 17.4, and 24.6 wt%, respectively, and the rest is graphite. Fig. 7c shows charge specific capacity within 20 cycles at 50 mA g^{-1}. It can be seen that Si/C-800-1 has the largest initial charge specific capacity of 654.6 mA h g^{-1}, possibly because of its high Si content. However, its specific capacity drops abruptly to 456.0 mA h g^{-1} after 20 cycles and the capacity retention becomes only 69.7% finally. Si/C-800-3 exhibits better cycle performance than Si/C-800-1, but delivers the lowest specific capacity of 427.9 mA h g^{-1}, because of the higher AC content in this sample. Therefore, in the Si/C composite, more Si leads to higher specific capacity but more carbon to better cycle stability. Compared to the above two samples, Si/C-800-2 has the intermediate content of GMs, Si, and AC, the highest specific capacity of 522.6 mA h g^{-1} and excellent cycle stability (its capacity retention is 98.8% after 20 cycles). It is clear that the contents of Si and AC significantly affect the specific capacity and cycling properties of Si/C composites. Fig. 7d shows the electrochemical impedance plots of these samples. The size of the semicircle, which indicates the resistance to charge transfer in the electrode, is much smaller for the Si/C-800-2 composite than the other samples, indicating its lower electrochemical reaction resistance, possibly due to the proper amount of AC incorporated as the conductive binder.

Fig. 8a shows the voltage profiles of Si/C-800-2 at different rates. Its charge specific capacity is 522.6 mA h g^{-1} at 50 mA g^{-1}, 510.0 mA h g^{-1} at 100 mA g^{-1}, 425.8 mA h g^{-1} at 200 mA g^{-1}, and 306.9 mA h g^{-1} at 500 mA g^{-1}. The charge specific capacity at 100 mA g^{-1} has 97.6% of that at 50 mA g^{-1}, indicating a superior rate capability between 50 mA g^{-1} and 100 mA g^{-1} Fig. 8b shows the rate performance of Si/C-800-2 and GMs. Highly stable and reversible capacities around 520, 510, 420, and 300 mA h g^{-1} are obtained at 50, 100, 200, and 500 mA g^{-1} respectively for Si/C-800-2. These values are much higher than those of GMs, e.g., it is 300 mA h g^{-1} for the former and 150 mA h g^{-1} for the later at 500 mA g^{-1}. The capacity retention of Si/C-800-2 after 20 cycles is 98.8, 98.6, 98.0 and 93.9% at 50, 100, 200, and 500 mA g^{-1}, respectively, comparable to those of GMs. Yang et al. [53] prepared Si/C composites with nanosized Si and fine graphite particles embedded in pyrolyzed carbon. At a current density of 125 mA g^{-1}, the initial specific capacity was about 700 mA h g^{-1}, and after 20 cycles, it still maintained near 680 mA h g^{-1}. The capacity retention of their samples was about 97.1%, slightly lower than 98.0% of Si/C-800-2 at 200 mA g^{-1}. Wen et al. [45] prepared Si/C composite by pyrolysis of pitch embedded with graphite and Si powders, which had an initial specific capacity of 800–900 mA h g^{-1} at the current density of 0.25 mA cm^{-2} (167 mA g^{-1}). After 20 cycles, the specific capacity became about 700 mA h g^{-1}, and the capacity retention was lower than 98.0% of Si/C-800-2 at 200 mA g^{-1} Fig. 8c shows the cyclic voltammogram curves of Si/C-800-2 for the first three cycles. Two distinct reductive peaks located between 0.75 and 0.20 V, and below 0.20 V respectively are identified, which correspond to the formation of the SEI film (0.20–0.75 V) and insertion of lithium ions into active materials respectively. The reductive peak between 0.75 and 0.20 V disappears in subsequent cycles. The oxidative peak, located at about 0.25 V is due to the extraction of lithium ions from graphite and de-alloying of Li_xSi. The reductive and oxidative peaks gradually become stronger and stronger with increase of the cycles, indicating its good cycle performance. These cyclic voltammogram characteristics are in good agreement with the galvanostatic charge–discharge profiles. According to the above characterization, the structure of the Si/C composite can be illustrated in Scheme 2. The Si particles are bound onto the surface of the GMs with AC as the conductive binder, which forms interconnection between GMs and Si particles [54,55]. Once the AC layer is

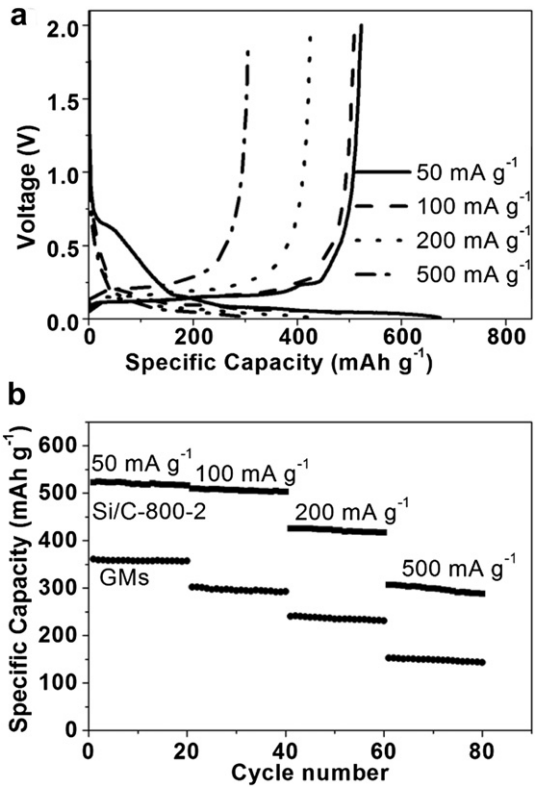

Fig. 8. (a) Galvanostatic charge-discharge profiles of Si/C-800-2 at different rates, (b) Rate performance of Si/C-800-2 and GMs, and (c) cyclic voltammogram of Si/C-800-2 at a scan rate of 0.1 mV s^{-1}.

formed, large Si/C particles are generated as shown in Fig. 5d. The GMs and AC acting as a coupling buffer matrix can prevent the adverse volume effect of the Si particles during the electrochemical cycling. In addition, the AC network can improve the electronic and ionic conductivity of the composite material [42,56], and facilitate the formation of stable SEI on the surface of Si [57], which will decrease the initial irreversible specific capacity [42]. For treatment at higher temperatures, it will lead to the formation of dense and hard carbon, which will be helpful to maintain the structural stability and accommodates the volume change of the Si particles during the charge and discharge cycles. However, the encapsulation of Si particles by the hard carbon will also result in loss in capacity as some of the Si particles will become inactive [58,59]. Considering all the aspects, it is understandable that 800 °C is the optimal carbonization temperature. Regarding the Si particles, probably a particle size at nanometer level is preferred, as it may reduce the mechanical stresses, shorten the Li diffusion distance [60], and

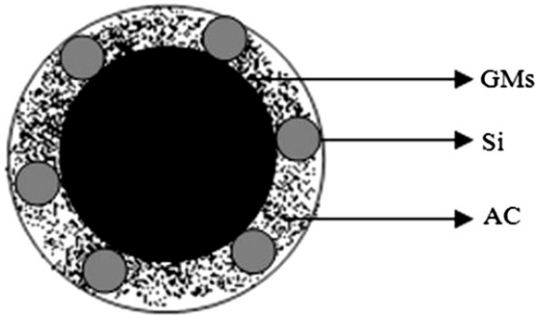

Scheme 2. Scheme of Si/C composite.

facilitate the rapid transport of Li ions [57]. The impurity in the Si particles may have negative effect on the electrochemical performance. The investigation on the influences of these factors is still undergoing.

4. Conclusions

In summary, we have fabricated novel Si/C anode composites composed of the commercial graphite microspheres (GMs), Si particles, and amorphous carbon (AC). Si particles are derived from solid Si waste of organosilane industry. AC is generated from sucrose and acts as a conductive binder. It is found that the capacity and cycling properties of the Si/C composites are related to the synthesis conditions such as carbonization temperatures and raw material ratio. The Si/C composite obtained at the optimal condition (800 °C and 5 h) contains 60.5 wt% of GMs, 22.1 wt% of the Si particles, and 17.4 wt% of the amorphous carbon, and shows the best electrochemical performance with a specific capacity of 522.6 mA h g^{-1} at 50 mA g^{-1} and 306.9 mA h g^{-1} at 500 mA g^{-1}, much higher than those of GMs. Meanwhile, the capacity retention of 93.9% at 500 mA g^{-1} after 20 cycles is also comparable to that of GMs. The work demonstrates the value-added utilization of low cost Si particles generated from the industrial solid Si waste to enhance commercial graphite anodes for Li-ion batteries.

Acknowledgment

The authors gratefully acknowledge the supports from National Natural Science Foundation of China (No. 51272252), Fund of State Key Laboratory of Multiphase Complex Systems (No. MPCS-2012-A-09), Hundred Talents Program of the Chinese Academy of Sciences, Priority Academic Program Development of Jiangsu Higher Education Institutions (PAPD) (No. SA1102), and the Fundamental Research Funds for the Central Universities (No. 2012LWB29).

References

[1] Y.-S. Hu, R. Demir-Cakan, M.-M. Titirici, J.-O. Müller, R. Schlögl, M. Antonietti, J. Maier, Angew. Chem. Int. Ed. 47 (2008) 1645–1649.
[2] R.A. Huggins, J. Power Sources 81–82 (1999) 13–19.
[3] C.K. Chan, H. Peng, G. Liu, K. Mcilwrath, X.F. Zhang, R.A. Huggins, Y. Cui, Nat. Nanotechnol. 3 (2008) 31–35.
[4] P. Gu, R. Cai, Y. Zhou, Z. Shao, Electrochim. Acta 55 (2010) 3876–3883.
[5] L.-F. Cui, R. Ruffo, C.K. Chan, H. Peng, Y. Cui, Nano Lett. 9 (2009) 491–495.
[6] W. Wang, P.N. Kumta, ACS Nano 4 (2010) 2233–2241.
[7] X.H. Liu, L. Zhong, S. Huang, S.X. Mao, T. Zhu, J.Y. Huang, ACS Nano 6 (2012) 1522–1531.
[8] Y. Liu, B. Chen, F. Cao, H.L.W. Chan, X. Zhao, J. Yuan, J. Mater. Chem. 21 (2011) 17083–17086.
[9] M. Thakur, M. Isaacson, S.L. Sinsabaugh, M.S. Wong, S.L. Biswal, J. Power Sources 205 (2012) 426–432.
[10] X. Li, P. Meduri, X. Chen, W. Qi, M.H. Engelhard, W. Xu, F. Ding, J. Xiao, W. Wang, C. Wang, J.-G. Zhang, J. Liu, J. Mater. Chem. 22 (2012) 11014–11017.
[11] X. Feng, J. Yang, P. Gao, J. Wang, Y. Nuli, RSC Adv. 2 (2012) 5701–5706.
[12] X. Wang, Z. Wen, Y. Liu, Electrochim. Acta 56 (2011) 1512–1517.
[13] H. Li, X. Huang, L. Chen, Z. Wu, Y. Liang, Electrochem. Solid-State Lett. 2 (1999) 547–549.
[14] W. Xu, S.S.S. Vegunta, J.C. Flake, J. Power Sources 196 (2011) 8583–8589.
[15] Z. Huang, R. Wang, D. Jia, L. Maoying, M.G. Humphrey, C. Zhang, ACS Appl. Mater. Interfaces 4 (2012) 1553–1559.
[16] T. Song, D.H. Lee, M.S. Kwon, J.M. Choi, H. Han, S.G. Doo, H. Chang, W.I. Park, W. Sigmund, H. Kim, U. Paik, J. Mater. Chem. 21 (2011) 12619–12621.
[17] Y. Yao, N. Liu, M.T. McDowell, M. Pasta, Y. Cui, Energy Environ. Sci. 5 (2012) 7927–7930.
[18] H. Chen, Y. Xiao, L. Wang, Y. Yang, J. Power Sources 196 (2011) 6657–6662.
[19] C.K. Chan, R.N. Patel, M.J. O'Connell, B.A. Korgel, Y. Cui, ACS Nano 4 (2010) 1443–1450.
[20] K. Peng, J. Jie, W. Zhang, S.-T. Lee, Appl. Phys. Lett. 93 (2008) 033105.
[21] T. Song, J. Xia, J.-H. Lee, D.H. Lee, M.-S. Kwon, J.-M. Choi, J. Wu, S.K. Doo, H. Chang, W.I. Park, D.S. Zang, H. Kim, Y. Huang, K.-C. Hwang, J.A. Rogers, U. Paik, Nano Lett. 10 (2010) 1710–1716.
[22] A. Gohier, B. Laïk, K.-H. Kim, J.-L. Maurice, J.-P. Pereira-Ramos, C.S. Cojocaru, P.T. Van, Adv. Mater. 24 (2012) 2592–2597.
[23] J. Shu, H. Li, R. Yang, Y. Shi, X. Huang, Electrochem. Commun. 8 (2006) 51–54.
[24] N.S. Hieu, J.C. Lim, J.K. Lee, Microelectron. Eng. 89 (2012) 138–140.
[25] J.P. Maranchi, A.F. Hepp, P.N. Kumta, Electrochem. Solid-State Lett. 6 (2003) A198–A201.
[26] M.D. Fleischauer, J. Li, M.J. Brett, J. Electrochem. Soc. 156 (2009) A33–A36.
[27] Y. Yao, M.T. McDowell, I. Ryu, H. Wu, N. Liu, L. Hu, W.D. Nix, Y. Cui, Nano Lett. 11 (2011) 2949–2954.
[28] H. Kim, B. Han, J. Choo, J. Cho, Angew. Chem. Int. Ed. 47 (2008) 10151–10154.
[29] H.-C. Shin, J.A. Corno, J.L. Gole, M. Liu, J. Power Sources 139 (2005) 314–320.
[30] C. Wang, L. Yin, D. Xiang, Y. Qi, ACS Appl. Mater. Interfaces 4 (2012) 1636–1642.
[31] S. Hossain, Y. Saleh, R. Loutfy, J. Power Sources 96 (2001) 5–13.
[32] A. Magasinski, P. Dixon, B. Hertzberg, A. Kvit, J. Ayala, G. Yushin, Nat. Mater. 9 (2010) 353–358.
[33] M.-H. Park, M.G. Kim, J. Joo, K. Kim, J. Kim, S. Ahn, Y. Cui, J. Cho, Nano Lett. 9 (2009) 3844–3847.
[34] H. Kim, M. Seo, M.-H. Park, J. Cho, Angew. Chem. Int. Ed. 49 (2010) 2146–2149.
[35] M. Holzapfel, H. Buqa, W. Scheifele, P. Novak, F.-M. Petrat, Chem. Commun. (2005) 1566–1568.
[36] R. Demir Cakan, M.-M. Titirici, M. Antonietti, G. Cui, J. Maier, Y.-S. Hu, Chem. Commun. (2008) 3759–3761.
[37] S.-H. Ng, J. Wang, D. Wexler, K. Konstantinov, Z.-P. Guo, H.-K. Liu, Angew. Chem. Int. Ed. 45 (2006) 6896–6899.
[38] L. Ji, X. Zhang, Energy Environ. Sci. 3 (2010) 124–129.
[39] L.-F. Cui, Y. Yang, C.-M. Hsu, Y. Cui, Nano Lett. 9 (2009) 3370–3374.
[40] W.-S. Chang, C.-M. Park, J.-H. Kim, Y.-U. Kim, G. Jeong, H.-J. Sohn, Energy Environ. Sci. 5 (2012) 6895–6899.
[41] E.G. Rochow, J. Am. Chem. Soc. 67 (1945) 963–965.
[42] P. Wang, Y. NuLi, J. Yang, Y. Zheng, Int. J. Electrochem. Sci. 1 (2006) 122–129.
[43] X. Yang, Z. Wen, X. Zhu, S. Huang, Electrochem. Solid-State Lett. 8 (2005) A481–A483.
[44] Y. Liu, T. Matsumura, N. Imanishi, A. Hirano, T. Ichikawa, Y. Takeda, Electrochem. Solid-State Lett. 8 (2005) A599–A602.
[45] Z.S. Wen, J. Yang, B.F. Wang, K. Wang, Y. Liu, Electrochem. Commun. 5 (2003) 165–168.
[46] J. Guo, A. Sun, X. Chen, C. Wang, A. Manivannan, Electrochim. Acta 56 (2011) 3981–3987.
[47] F. Su, J. Zeng, Y. Yu, L. Lv, J.Y. Lee, X.S. Zhao, Carbon 43 (2005) 2366–2373.
[48] B. Philippe, R. Dedryvère, J. Allouche, F. Lindgren, M. Gorgoi, H. Rensmo, D. Gonbeau, K. Edström, Chem. Mater. 24 (2012) 1107–1115.
[49] Z. Zhang, H. Che, J. Gao, Y. Wang, X. She, J. Sun, P. Gunawan, Z. Zhong, F. Su, Catal. Sci. Technol. 2 (2012) 1207–1212.
[50] P. Zuo, Z. Wang, G. Yin, D. Jia, X. Cheng, C. Du, P. Shi, J. Mater. Sci. 43 (2008) 3149–3152.
[51] V.G. Khomenko, V.Z. Barsukov, Electrochim. Acta 52 (2007) 2829–2840.
[52] R. Ruffo, S.S. Hong, C.K. Chan, R.A. Huggins, Y. Cui, J. Phys. Chem. C 113 (2009) 11390–11398.
[53] J. Yang, B.F. Wang, K. Wang, Y. Liu, J.Y. Xie, Z.S. Wen, Electrochem. Solid-State Lett. 6 (2003) A154–A156.
[54] K. Wang, R. Cai, T. Yuan, X. Yu, R. Ran, Z. Shao, Electrochim. Acta 54 (2009) 2861–2868.
[55] W. Xing, J.S. Xue, J.R. Dahn, J. Electrochem. Soc. 143 (1996) 3046–3052.
[56] M. Yoshio, H. Wang, K. Fukuda, T. Umeno, N. Dimov, Z. Ogumi, J. Electrochem. Soc. 149 (2002) A1598–A1603.
[57] Y.-X. Yin, S. Xin, L.-J. Wan, C.-J. Li, Y.-G. Guo, J. Phys. Chem. C 115 (2011) 14148–14154.
[58] I.-S. Kim, P.N. Kumta, J. Power Sources 136 (2004) 145–149.
[59] X.-W. Zhang, P.K. Patil, C. Wang, A.J. Appleby, F.E. Little, D.L. Cocke, J. Power Sources 125 (2004) 206–213.
[60] B.-C. Kim, H. Uono, T. Sato, T. Fuse, T. Ishihara, M. Senna, Solid State Ionics 172 (2004) 33–37.